

ADAPTIVE VERTICAL SEISMIC ISOLATION FOR EQUIPMENT

ADAPTIVE VERTICAL SEISMIC ISOLATION FOR EQUIPMENT

By MOHAMMADREZA NAJAFIJOZANI, M.SC., B.SC.

A Thesis Submitted to the School of Graduate Studies in Partial Fulfilment of the
Requirements for the Degree Master of Applied Science

McMaster University ©Copyright by Mohammadreza Najafijozani, May 2019

MASTER OF APPLIED SCIENCE (2019)

McMaster University

(Civil Engineering)

Hamilton, Ontario

Title: ADAPTIVE VERTICAL SEISMIC ISOLATION FOR EQUIPMENT

AUTHOR: MOHAMMADREZA NAJAFIJOZANI, M.Sc. (Iran University of Science
and Technology, Tehran, Iran)

SUPERVISOR: Dr. Michael Tait

NUMBER OF PAGES: x, 60

ABSTRACT

Nuclear power plants (NPP) house a large number of acceleration-sensitive equipment. To protect this equipment during earthquakes, researchers have proposed implementing seismic isolation in the horizontal direction and even in the vertical direction. For traditional horizontal isolation, adaptive systems have been developed to achieve different performance objectives under a range of earthquake levels. However, this multiple performance approach has not been adopted in designing vertical isolation devices. This paper investigates the feasibility of an adaptive vertical isolation system for equipment. Three different system are investigated: linear spring and linear damper (LSLD), linear spring and nonlinear damper (LSND) and nonlinear spring and linear damper (NSLD). All of these systems are designed to meet the performance goals in each hazard level. Thirty triaxial ground motions are selected and scaled separately in horizontal and vertical directions. Nonlinear dynamic analysis is conducted for a nuclear power plan archetype in Diablo Canyon site in California representing high-level seismicity. The floor motions at the location of the equipment are used as seismic input to the equipment. The performance of the systems is evaluated based on the peak equipment acceleration, average spectral acceleration in the range 5-33 Hz and maximum displacement of isolation system. The results illustrate that equipment in the LSND system experience superior protection in the vertical direction.

ACKNOWLEDGEMENT

I would like to express my deepest gratitude to my supervisors, Dr. Konstantinidis and Dr. Becker for their consistent support and guidance during this research. I am also grateful to Dr. Tait and Dr. El-Dakhankhni for their help and support throughout this research. I would like to thank Sarah Sullivan and Beth Bierema, the staff of the Civil Engineering department.

Thank you to my dearest friends Mehdi Shafikhani and Hossein Mohammadi. I need to appreciate my mom, to whom I owe everything. Finally, I need to thank myself. Without myself, this project would not have been done.

TABLE OF CONTENTS

Chapter 1 INTRODUCTION.....	1
1.1 Introduction	1
1.2 Research objectives	5
1.3 Thesis organization	5
1.4 References	6
Chapter 2 ADAPTIVE VERTICAL SEISMIC ISOLATION FOR EQUIPMENT	8
Abstract	8
2.1 Introduction	9
2.2 Nuclear power plant structure and component of interest.....	12
2.2.1 Nuclear power plant internal structure model	12
2.2.2 Design spectra.....	13
2.2.3 Horizontal base isolation of the superstructure	15
2.2.4 Ground motion selection and scaling	18
2.3 Equipment of interest	20
2.4 Performance objectives	20
2.4.1 Equipment.....	21
2.4.2 Vertical seismic isolation system	23
2.5 Vertical seismic isolation systems.....	24
2.5.1 Linear spring and linear damper.....	26
2.5.2 Linear spring and nonlinear damper	28
2.5.3 Nonlinear spring and linear damper	30
2.6 Results: comparison of the vertical isolation systems.....	34
2.7 Discussion: Adaptive behavior in horizontal and vertical direction	38
2.8 Conclusions	40
References	42
Chapter 3 CONCLUSIONS AND RECOMMENDATIONS.....	48
3.1 Summary	48
3.2 Conclusion.....	49
3.3 Recommendation and future study.....	50

APPENDIX A.....	52
APPENDIX B.....	57
References.....	60

LIST OF FIGURES

Figure 1-1:	3D isolation system including ball bearing, coil spring, and air spring [3]	2
Figure 1-2:	3D isolation system including multi-stage rubber bearing and coil spring and damper [4]-----	2
Figure 1-3:	3D isolation including spring and damper [6] -----	3
Figure 2-1:	Lumped mass stick model of NPP showing the location of the motor control center (MCC)-----	13
Figure 2-2:	Horizontal (left) and vertical (right) target and mean response spectra (DBE level) -----	14
Figure 2-3:	Force-displacement relation of the LRB in the horizontal direction-----	15
Figure 2-4:	Force-displacement relation of the LRB in the vertical direction-----	18
Figure 2-5:	Motor control center (MCC) -----	20
Figure 2-6:	The fragility curves of failure modes of MCC: contact chatter voltage drop-out (CCVD), change of state of starter auxiliary contact (CSSAC), and change of state of starter main contact (CSSMC)-----	23
Figure 2-7:	(Left) Vertical ground and floor acceleration spectra at the location of the equipment, (right) Vertical ground and floor displacement spectra at the location of the equipment at DBE level (The right figure also shows the displacement demand at 1.8 Hz which is the selected frequency of the LSLD system).-----	25
Figure 2-8:	(Left) Vertical ground and floor acceleration spectra at the location of the equipment, (right) Vertical ground and floor displacement spectra at the	

location of the equipment at BDBE level (The right figure also shows the displacement demand at 1.8 Hz which is the selected frequency of the LSLD system).----- 26

Figure 2-9: Nonlinear springs configurations with force displacement relation (Black arrows show static equilibrium).----- 31

Figure 2-10: Different effective characteristics at DBE level with softening and hardening region ----- 33

Figure 2-11: Comparison of the elastic spring behavior of the vertical isolation systems (u is dynamic displacement and d is total displacement). ----- 35

Figure 2-12: Left: Vertical response spectra for the equipment. Right: maximum total displacement of the isolation systems at the DBE level. (Black circles show the static displacement) ----- 36

Figure 2-13: Left: Vertical response spectra for the equipment. Right: maximum total displacement of the isolation systems at the BDBE level. (Black circles show the static displacement) ----- 37

Figure 2-14: (Left) Acceleration spectra and (right) displacement spectra for horizontal direction on the ground and for vertical direction at the location of the MCC. T_H and T_V shows examples of effective horizontal and vertical isolation systems. (The damping ratio is 5%). ----- 39

LIST OF TABLES

Table 2-1:	Design parameters of an individual LRB -----	15
Table 2-2:	Selected ground motions with horizontal and vertical scale factors (SF_H and SF_V are scale factor in horizontal and vertical direction, respectively. M is the magnitude of earthquake and r is the distance to the rupture plane and V_{S30} is the average shear velocity of top 30 m.) -----	19
Table 2-3:	Performance expectations for seismically isolated structure [33]-----	21
Table 2-4:	Fragility parameters of failure modes of the MCC [31] -----	23
Table 2-5:	Design parameter of each helical spring -----	28
Table 2-6:	The design properties of three systems -----	35
Table 2-7:	The summary results of the peak base acceleration and the displacement of the four systems. (Bold numbers exceed the performance goal) -----	38
Table A-1:	Nodes of internal structure (lumped mass) -----	52
Table A-2:	Nodes of internal structure (stick) -----	53
Table A-3:	Three translational and three rotational mass components of each node -	54
Table A-4:	Geometric characteristics of beams and columns -----	55
Table A-5:	Rigid link elements -----	56
Table B-1:	Calculation of design parameters of the LRB-----	59

Chapter 1 INTRODUCTION

1.1 Introduction

Base isolation is a well-known strategy to mitigate the horizontal seismic responses for both structural and non-structural components. However, the vertical component of ground motion is transmitted through the superstructure and often amplified by the isolation systems. Efforts to evaluate the performance of conventional isolation systems in the vertical direction have been made at E-Defence laboratory in Japan. Furukawa et al. [1] conducted a full scale shaking table test of a four-story building. The medical facilities were used as contents of the building. In general, the isolation system could not reduce the vertical responses and significant damages were observed in this equipment due to vertical ground shaking.

Japanese researchers proposed three-dimensional isolation systems for the use in power plants. Lee and Constantinou [2] summarized these systems and explained the horizontal and vertical characteristics of each system. Tsutsumi et al. [3] proposed an isolation system consisting of a ball bearing and a coil spring for the horizontal isolation and air spring and viscous damper for the vertical isolation (Figure 1-1). The vertical frequency of this system was measured experimentally to be 1.06 Hz. The main problem of this system was large static deflection. Tsutsumi et al. [4] proposed another system including multi-stage elastomeric bearings for horizontal isolation and coil springs and dampers for vertical isolation (Figure 1-2). The vertical frequency of this system was 2 Hz. The complexity and the total height of this system were the main problems of this system.

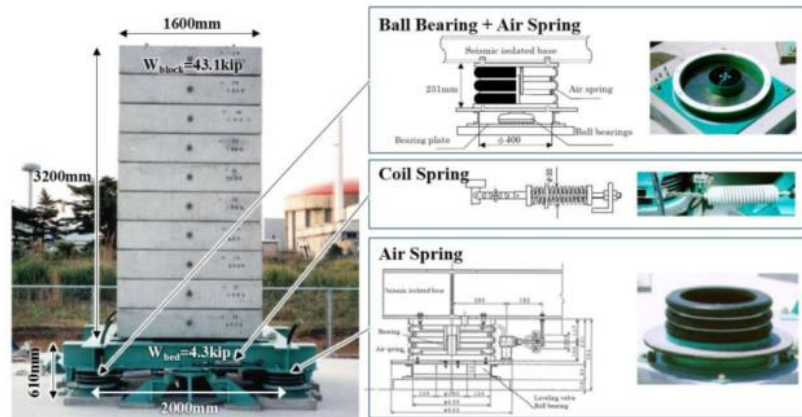


Figure 1-1: 3D isolation system including ball bearing, coil spring, and air spring [3]



Figure 1-2: 3D isolation system including multi-stage rubber bearing and coil spring and damper [4]

In general, there are three separate approaches in providing 3D isolation. The first approach is to provide 3D isolation at the base between the superstructure and the foundation. The example of the first approach is the Chisuikan residential apartment that was built in 2011

[5]. The isolation system includes the elastomeric bearing for horizontal isolation and vertical air springs and dampers for vertical isolation. The vertical frequency is 0.77 Hz and horizontal frequency is 0.43 Hz. The system is complex and needs a rocking suppression system.

The second approach is to isolate the equipment in horizontal and vertical directions between the equipment and the floor. The isolation system can significantly reduce the vertical acceleration transmitted to the equipment. Nawrotzki and Siepe [6] investigated an integrated elastic 3D isolation system consisting of helical springs and viscous dampers to protect emergency diesel generators and emergency power system (Figure 1-3). The springs were flexible in both the horizontal and vertical directions. They showed that the system improved significantly the seismic performance of the equipment. However, they recommended checking the vertical displacement to avoid any damage to the springs.

Lee and Constantinou [7] proposed two 3D isolation systems designed for power transformers. The first system was a horizontal-vertical integrated isolation system consisting of coil springs with an inclined linear viscous damper, and the second one was



Figure 1-3: 3D isolation including spring and damper [6]

a system which consisted of a TFP system for horizontal isolation and coil springs with a viscous damper within a telescopic system for the vertical direction. The study concluded that rocking was a concern for the first system and the performance of the second system was more effective in attenuating acceleration response. However, the study also cautioned that the second system may become ineffective for certain ground motions. Specifically, when the vertical frequency of the isolation system was 1.5-2.0 Hz, the seismic response remained unchanged or was amplified for ground motions with strong vertical and horizontal components in the 1.5-3.0 Hz range.

The third approach is to isolate the whole superstructure at the base horizontally and the equipment at the attached location vertically. Medel-Vera and Ji [8] concluded that the third approach is more appealing because no rocking suppression system is required, there is no coupling between the horizontal and vertical isolation systems, and it may be more practical for maintenance purposes. Additionally, the weight of targeted equipment is very low compared to the entire superstructure, making the implementation of the vertical isolation practically more feasible. As such, the third approach is explored in this research.

Recently, adaptive behavior in horizontal base isolation systems has been proposed to meet multiple objectives under increasing levels of ground motion excitation. The adaptability of these systems is derived from the physical configuration of the systems. The focus of this research is to investigate the adaptive vertical isolation systems for equipment.

1.2 Research objectives

The main objective of this research is to investigate the potential benefits of adaptive equipment isolation system in the vertical direction. The study examines the experimental fragility curves of a specific acceleration-sensitive equipment in NPP to determine the failure modes. The engineering demand parameter value corresponding to each performance objectives is determined from the corresponding fragility curves. Three systems are proposed: linear spring and linear damper (LSLD), linear spring and nonlinear damper (LSND), and nonlinear spring and linear damper (NSLD). The designs of these systems, aimed to capture multiple performance goals in different hazard levels, are presented.

The scope of thesis includes ascertaining acceleration demands on the equipment by comparing the response spectra at the floor level for fixed-based equipment and at the top of the isolation system for isolated equipment. The performance of three systems are evaluated by studying the peak spectral acceleration, the average spectral acceleration in the frequency range 5-33 Hz, and the maximum displacement of the isolation system.

1.3 Thesis organization

The thesis is organized in three chapters. Chapter 2 presents the contents of the following article:

Najafijozani M, Konstantinidis D, Becker T. “Adaptive vertical seismic isolation for equipment in nuclear power plants.” To be submitted to *Nuclear Engineering and Design*.

Chapter 3 presents the summary, conclusion and topics for future research. There are two appendices:

- 1) Appendix A contains the coordinates of the lumped mass and stick model, the translational and rotational masses values at each node, and the geometric characteristics of the sections of beams and columns.
- 2) Appendix B contains the process of design of the lead rubber bearing (LRB) for the horizontal isolation of superstructure.

1.4 References

- [1] Furukawa, S., Sato, E., Shi, Y., Becker, T. and Nakashima, M. (2013). “Full-scale shaking table test of a base-isolated medical facility subjected to vertical motions.” *Earthquake Engineering & Structural Dynamics*, 42(13):1931-49.
- [2] Lee, D. and Constantinou, M. (2017). *Development and Validation of Combined Horizontal-Vertical Seismic Isolation System for High-Voltage Power Transformers*. Report No. MCEER-17-0007, Multidisciplinary Center for Earthquake Engineering Research, University at Buffalo, USA.
- [3] Tsutsumi, H., Yamada, H., Mori, K., Ebisawa, K. and Shibata, K. (2000). *Characteristics and dynamic response of 3-D component base isolation system using ball bearings and air springs*. Report No. JAERI-Tech 2000-086 in Japanese, Japan Atomic Energy Research Inst., Japan.

- [4] Tsutsumi, H., Yamada, H., Ebisawa, K., Shibata, K. and Fujimoto, S. (2001). *Shaking table test and dynamic response analysis of 3-D component base isolation system using multi-layer rubber bearings and coil springs*. Report No. JAERI-Tech 2001-033 in Japanese, Japan Atomic Energy Research Inst., Japan.
- [5] Mori, S., Suhara, I., Saruta, M., Okada, K., Tomizawa, T., Tsuyuki, Y., et al. (2012).“Simulation analysis of free vibration test in a building Chisuikan using three-dimensional seismic base isolation system.” *15th World conference on earthquake engineering*, Lisbon, Portugal.
- [6] Nawrotzki, P. and Siepe, D. (2014).“Structural Challenges of power plants in high seismic areas.” *Second European Conference on Earthquake Engineering and Seismology*, Istanbul, Turkey.
- [7] Lee, D. and Constantinou, M. C. (2018). “Combined horizontal–vertical seismic isolation system for high-voltage–power transformers: development, testing and validation.” *Bulletin of Earthquake Engineering*:1-24.
- [8] Medel-Vera, C. and Ji, T. (2015). “Seismic protection technology for nuclear power plants: a systematic review.” *Journal of Nuclear Science and Technology*, 52(5):607-32.

Chapter 2 ADAPTIVE VERTICAL SEISMIC ISOLATION FOR EQUIPMENT

This chapter has the contents of the following article:

Najafijozani M, Konstantinidis D, Becker T. “Adaptive vertical seismic isolation for equipment in nuclear power plants.” To be submitted to *Nuclear Engineering and Design*.

Abstract

Seismic isolation systems are widely recognized as beneficial for protecting both acceleration- and displacement-sensitive nonstructural systems and components. Furthermore, adaptive isolation systems have been shown to enable engineers to achieve various performance goals under multiple hazard levels. These systems have been implemented for horizontal excitation, but there has been very limited research on isolation for vertical excitation. Thus, this paper seeks to evaluate the benefit of adaptive vertical isolation systems for component isolation, specifically for nuclear plants. To do this, three vertical isolation systems are designed to achieve multiple goals: a linear spring and a linear damper (LSLD), a linear spring and a nonlinear damper (LSND) and a nonlinear spring and a linear damper (NSLD). To investigate the effectiveness of the proposed systems, a stiff piece of equipment is considered at an elevated floor within a power plant. A set of 30 triaxial ground motions is used to investigate the seismic response of the equipment. The maximum isolation displacement and equipment acceleration are used to assess the effectiveness of the three isolation systems. While all systems significantly reduce the

seismic accelerations on the equipment compared to the fixed-base case, a LSND system is shown to exhibit superior seismic performance across multiple hazard levels.

2.1 Introduction

The protection of nuclear power plants (NPP) in seismic events is crucial, and isolation can be an effective tool to help achieve acceptable performance. For example, in the 2011 Tohoku-Oki megathrust earthquake, the base-isolated emergency building in the Fukushima Daiichi plant performed well [1], spurring more research on protective systems for nuclear power plants. Several studies [2-6] have investigated the effectiveness of base isolation in NPP. The focus of these studies has predominantly been for horizontal isolation. Despite the effectiveness of traditional isolation in reducing the horizontal seismic response of equipment, conventional seismic isolation systems are stiff in the vertical direction and thus do not reduce the vertical seismic response. Whittaker et al. [7] concluded that, while base isolation could significantly decrease the horizontal demand in NPPs, the vertical response was the same as for the fixed base NPP. This has also been experimentally observed. In a shake table test study of a full-scale medical facility at E-Defense, Furukawa et al. [8] found that while the isolation system effectively reduced the horizontal accelerations, the vertical accelerations were amplified between the ground and the floor above the isolation layer by a factor of 1.5 and from there to the top floor by another 1.5, causing notable nonstructural content damage. In a separate full-scale test at E-Defense, Guzman Pujols and Ryan [9] observed that the vertical peak floor acceleration in an isolated structure with lead rubber bearings (LRB) was amplified from 2 g at the second floor to 7 g at the roof. This is compounded by large vertical components of input

motions that have been underestimated for near field sites. Papazoglou and Elnashai [10] found that in multiple earthquakes, for near-fault locations, both structural and nonstructural damage was significantly influenced by the vertical ground motion components.

To address the shortcoming of conventional isolation systems in controlling vertical accelerations, there have been attempts to provide effective 3D seismic isolation. In general, there are three approaches for 3D isolation: (1) to use 3D isolation for the whole structure at its base, (2) to use 3D isolation just for the equipment, and (3) to use horizontal isolation at the base of structure and vertical isolation for the equipment only. An example of the first approach is the Chisuikan residential apartment building, constructed in 2011 in Japan? [11]. The isolation system includes elastomeric bearings for horizontal isolation and vertical air springs and dampers for vertical isolation; however, the flexible vertical system at the base necessitates a vertical rocking suppression system.

Using the second approach, Nawrotzki and Siepe [12] used helical springs, flexible in both the horizontal and vertical directions, and viscous dampers, to protect emergency diesel generators and emergency power system. While the authors noted a significant improvement in the seismic performance of the equipment, they recommended to the designers to check the vertical displacement to avoid any damage to the springs. Lee and Constantinou [13] proposed two 3D isolation systems designed for power transformers. The first system was a horizontal–vertical integrated isolation system consisting of coil springs with an inclined linear viscous damper, and the second one was a system which consisted of a triple friction pendulum system for horizontal isolation and coil springs with

a viscous damper within a telescopic system for the vertical direction. The study concluded that rocking was a concern for the first system, and that the performance of the second system was more effective in attenuating acceleration response. However, the study also cautioned that the second system may amplify the vertical response for ground motions with high frequency content.

Medel-Vera and Ji [14], who conducted a systematic review of seismic isolation for NPP, concluded that the third approach in which the entire structure is isolated horizontally at the base and only individual equipment is vertically isolated is more appealing for NPP because no rocking suppression system is required, there is no coupling between the horizontal and vertical isolation systems, and it may be more practical for maintenance. Additionally, the weight of the targeted equipment is very low compared to the entire NPP superstructure, making the implementation of the vertical isolation practically more feasible.

For horizontal isolation systems, adaptive behavior has been proposed to meet multiple objectives under increasing levels of ground motion excitation [15]. The adaptability of these systems is derived from the physical configuration or material properties of the systems. However, research in adaptive vertical isolation systems is still new. Cimellaro et al. [16], Meng et al. [17], and Zhou et al. [18] studied the application of negative or quasi-zero stiffness devices proposed for vertical vibration mitigation for light, sensitive equipment. Ueda et al. [19] and Wakabayashi et al. [20] proposed bilinear vertical isolation systems which use multiple springs in parallel in an effort to reduce the static displacement and displacement under low-level earthquakes.

Thus, this paper investigates the potential benefits of adaptive vertical isolation systems for acceleration sensitive equipment in NPP. To this end, three systems are studied: a linear spring and a linear damper (LSLD), a linear spring and nonlinear damper (LSND), and a nonlinear spring with a linear damper (NSLD). Design methodologies for the vertical isolation systems are presented with the performance goals of the equipment in mind, and the performance of three systems are compared.

2.2 Nuclear power plant structure and component of interest

The effectiveness of the various vertical isolation systems on the seismic performance of a piece of equipment is evaluated in a representative NPP structure that is isolated horizontally at the base. This section discusses the superstructure and horizontal base isolation model of the NPP, as well as the design spectra, and the suite of ground motions used in the response history analysis of the NPP. The selected equipment, its performance objectives, and the vertical isolation systems considered are presented in subsequent sections.

2.2.1 Nuclear power plant internal structure model

The internal structure of the NPP is represented by a simplified 3D lumped-mass stick model [21], which is adapted in OpenSees [22] for the purposes of this study, as shown in Figure 2-1. The node coordinates, masses, and element stiffnesses are presented in Appendix A. The lumped mass nodes are connected to the internal structure by rigid elements. The total mass of internal structure is 50,000 ton. The height of internal structure is 39 m. Eigenvalue analysis of the fixed-base model shows that the natural frequencies of the first and second modes are 7.14 Hz (0.14 s) and 7.69 Hz (0.13 s), respectively. The

frequency of the twelfth mode of the superstructure, which is the first vertical mode, is 21.14 Hz (0.0473 s). The first twenty modes are verified with SAP2000 [23]. Rayleigh damping is used with 5% damping for the first and twelfth modes. Further information about the internal structure can be found in Huang et al. [24], who used the same internal structure model.

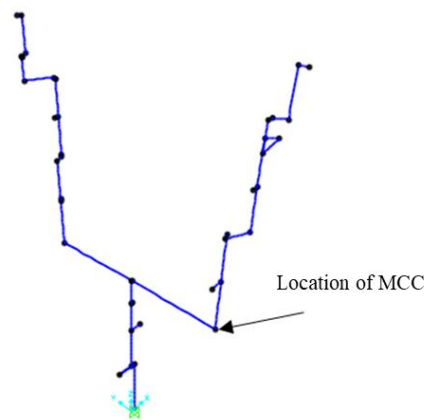


Figure 2-1: Lumped mass stick model of NPP showing the location of the motor control center (MCC)

2.2.2 Design spectra

The NPP is assumed to be at the Diablo Canyon, California, site. The provisions outlined in ASCE 43-05 [25] were used to determine the horizontal design response spectra for the design basis earthquake (DBE) with a return period of 10,000 years. The design response spectrum is found by multiplying the uniform hazard response spectra by the design factor. The design factor is the maximum of DF_1 and DF_2 [25]. Table 2-1 in ASCE 43-05 [25] specifies the value of $DF_1 = 1$ for seismic design category 5, which NPP belongs to. The second design factor is

$$DF_2 = 0.6(A_R)^\beta \tag{1}$$

where β is 0.8 for seismic design category 5 [25], and

$$A_R = \frac{SA_{0.1H_D}}{SA_{H_D}} \tag{2}$$

where SA_{H_D} is the spectral acceleration at the mean annual frequency of exceedance H_D , $SA_{0.1H_D}$ is the spectral acceleration at the mean annual frequency of exceedance $0.1H_D$, and H_D is 1×10^{-4} . DF_2 is less than one across all frequencies, and since $DF_1 = 1$, the design factor is taken as 1. The vertical to horizontal pseudo acceleration ratio recommended by ASCE 43-05 is used to determine the vertical design response spectra. This ratio is $2/3$ at frequencies below 3 Hz, one for frequencies above 5 Hz, and transitions from $2/3$ to 1 for frequencies between 3 Hz and 5 Hz. Figure 2-2 shows the horizontal and vertical DBE spectra with solid black lines.

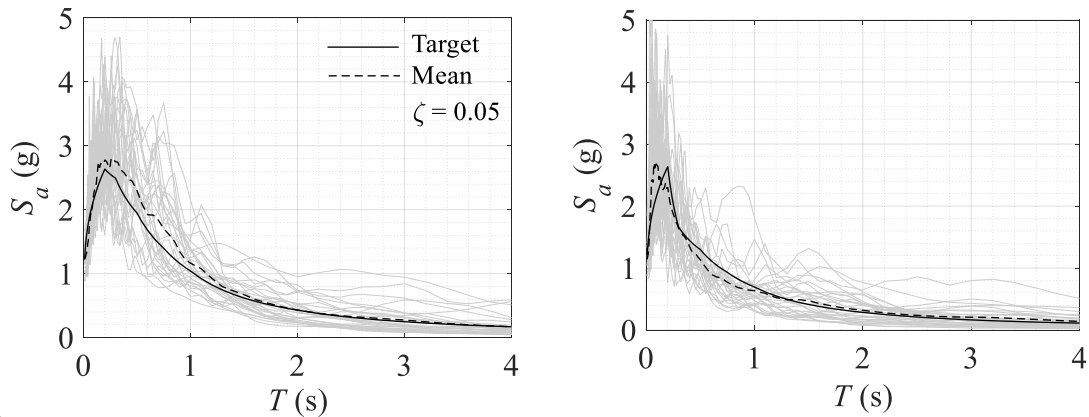


Figure 2-2: Horizontal (left) and vertical (right) target and mean response spectra (DBE level)

2.2.3 Horizontal base isolation of the superstructure

A horizontal isolation system with effective period and damping ratio of 2.5 s and 20%, consisting of 150 LRBs, is designed for the horizontal isolation at the base of the NPP. Table 2-1 summaries the design parameters of each LRB. Further details can be found in Appendix B. The force-displacement relation of the LRB is shown in Figure 2-3.

Table 2-1: Design parameters of an individual LRB

Design parameter	Value	Design parameter	Value
d (displacement demand)	0.5 m	σ (static pressure)	3 MPa
d_y (yielding displacement)	0.027 m	σ_L (yield strength of the lead)	8.5 MPa
Q_d (characteristic strength)	343 kN	D (diameter)	1.178 m
K_2 (post yield stiffness)	1,404 kN/m	D_L (diameter of lead plug)	0.22 m
H (height of the LRB)	0.56 m	S (shape factor)	20
K (bulk modulus)	2,000 MPa	G (shear modulus)	0.4 MPa
t_r (thickness of rubber)	34 cm		

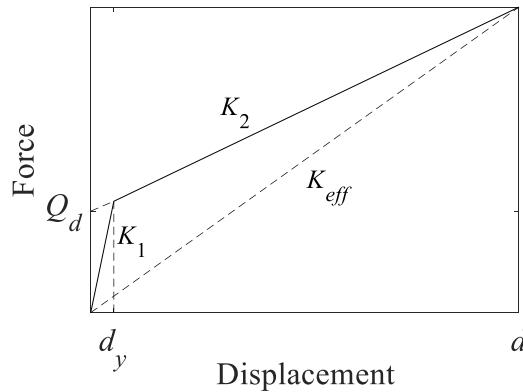


Figure 2-3: Force-displacement relation of the LRB in the horizontal direction

The post-yield stiffness of the LRB in the horizontal direction is [26]

$$K_2 = f_L \frac{GA}{t_r} \quad (3)$$

where G is the shear modulus of the elastomer, A is the area of the bearing, t_r is the total thickness of the rubber, and f_L is an experimental parameter for the effect of lead on the post-yield stiffness, taken as between 1.0 to 1.2 [26]. Here, this parameter is assumed to be 1.1.

The vertical stiffness of the LRB in compression is determined from

$$K_V = \frac{E_c A}{t_r} \quad (4)$$

where E_c is the compression modulus, which for an annular pad is given by [27, 28]

$$E_c = K [1 + C_1 (I_1(\vartheta) - \eta I_1(\eta\vartheta)) + C_2 (K_1(\vartheta) - \eta K_1(\eta\vartheta))] \quad (5)$$

where K is the bulk modulus, S is the shape factor, $\eta = D_L / D$, and

$$\vartheta = \sqrt{\frac{48G}{K} \frac{S}{1-\eta}} \quad (6)$$

and

$$C_1 = \frac{1}{\sqrt{\frac{12G}{K}} (1+\eta) S} \frac{K_0(\vartheta) - K_0(\eta\vartheta)}{I_0(\vartheta) K_0(\eta\vartheta) - I_0(\eta\vartheta) K_0(\vartheta)} \quad (7)$$

$$C_2 = \frac{1}{\sqrt{\frac{12G}{K}} (1+\eta) S} \frac{I_0(\vartheta) - I_0(\eta\vartheta)}{I_0(\vartheta) K_0(\eta\vartheta) - I_0(\eta\vartheta) K_0(\vartheta)} \quad (8)$$

where I_0 and I_1 are modified Bessel functions of the first kind and order 0 and 1, and K_0 and K_1 are modified Bessel functions of the second kind and order 0 and 1. With $G = 0.4$ MPa, $S = 20$, and $\eta = 0.2$, the compression modulus, is $E_c = 2.9GS^2$.

Rearranging Equations (3) and (4) leads to

$$K_V = \frac{2.9 S^2}{f_L} K_2 \quad (9)$$

Substituting in the values for S and f_L gives $K_V/K_2 = 1160$.

A bilinear elastic model was used to capture the reduction in stiffness that occurs when the rubber experiences cavitation in tension. Gent [29] proposed that the onset of cavitation occurs at negative pressure of $3G$. Hence, the cavitation strain is $3G/E_c = 3G/2.9GS^2 = 2.5 \times 10^{-3}$ (Figure 2-4). The post-cavitation force in this study is assumed to be constant. Damping in the LRB isolators in the vertical direction is neglected.

Modal analysis shows that the first six fundamental frequencies are 0.398 Hz (horizontal), 0.399 Hz (horizontal), 8.62 Hz (rotational), 8.66 Hz (torsional), 9.16 Hz (rotational) and 10.42 Hz (vertical). Without considering the effect of vertical stiffness of the LRB system, the first mode in the vertical direction is the twelfth mode which is at 21.16 Hz. Consequently, the effect of vertical stiffness of the dynamics of the LRB-isolated NPP is not negligible and therefore is accounted for in the analysis. The effect of lateral displacement on the vertical stiffness of an LRB is not considered in this study.

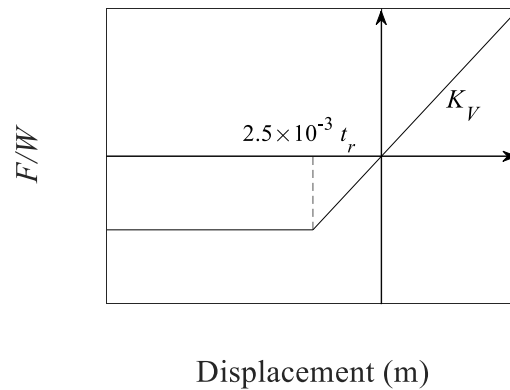


Figure 2-4: Force-displacement relation of the LRB in the vertical direction

2.2.4 Ground motion selection and scaling

To evaluate the performance of the different equipment vertical isolation systems, presented in a subsequent section, thirty ground motions are selected and scaled in the range from $0.2T_f$ to $1.5T_b$ [30], where T_f and T_b are the fundamental periods of the fixed-base and base-isolated NPP. Table 2-2 lists the suite of ground motions used in this study. The fundamental periods of fixed-base NPP are 0.14 s and 0.0473 s in the horizontal and vertical directions, respectively. The fundamental periods of base isolated NPP are assumed 2.5 s and 0.09 s in the horizontal and vertical directions, respectively. Hence, the scaling ranges are from 0.03 to 3.75 s for the horizontal ground motions and 0.001 to 0.15 s for the vertical ground motions. The scale factors for the horizontal and vertical direction are considerably different. Figure 2-2 show with grey lines the mean response spectra of the ground motions in the horizontal and vertical directions.

Table 2-2: Selected ground motions with horizontal and vertical scale factors (SF_H and SF_V are scale factor in horizontal and vertical direction, respectively. M is the magnitude of earthquake and r is the distance to the rupture plane and V_{S30} is the average shear velocity of top 30 m.)

No	Year	Earthquake Name	M	r (km)	V_{S30} (m/sec)	SF_H	SF_V
1	1935	Helena_Montana-01	6.1	2.86	593	6.21	10.84
2	1971	San Fernando	6.6	22.63	450	3.85	6.93
3	1976	Friuli_Italy-01	6.5	15.82	505	3.32	4.69
4	1978	Tabas_Iran	7.3	13.94	471	2.82	5.591
5	1979	Imperial Valley-06	6.5	15.19	471	5.14	6.59
6	1980	Mammoth Lakes-01	6.1	15.46	537	3.01	7.09
7	1980	Victoria_Mexico	6.3	14.37	471	1.97	4.05
8	1980	Irpinia_Italy-01	6.9	10.84	382	3.01	4.83
9	1981	Corinth_Greece	6.6	10.27	361	4.08	7.95
10	1984	Morgan Hill	6.2	0.53	561	1.25	2.68
11	1986	N. Palm Springs	6.1	14.24	388	8.77	13.66
12	1987	New Zealand-02	6.6	16.09	551	4.10	6.81
13	1989	Loma Prieta	6.9	10.72	476	1.76	2.34
14	1989	Loma Prieta	6.9	3.85	462	2.09	2.72
15	1992	Cape Mendocino	7.1	6.96	567	0.78	1.76
16	1994	Northridge-01	6.7	8.44	380	1.22	2.73
17	1994	Northridge-01	6.7	5.19	370	1.51	2.26
18	1999	Kocaeli_Turkey	7.5	13.49	523	5.98	10.54
19	1999	Chi-Chi_Taiwan	7.6	5.95	454	5.36	6.71
20	1999	Chi-Chi_Taiwan	7.6	7.08	468	2.12	3.42
21	1990	Manjil_Iran	7.3	12.55	723	1.59	1.92
22	2000	Tottori_Japan	6.6	9.12	616	4.60	8.27
23	2004	Parkfield-02_CA	6.1	2.57	397	3.59	9.46
24	2004	Parkfield-02_CA	6.1	9.47	466	4.44	6.29
25	2004	Niigata_Japan	6.6	9.46	480	1.27	2.86
26	2004	Niigata_Japan	6.6	8.93	375	1.85	4.31
27	2009	L'Aquila_Italy	6.3	6.27	475	1.78	2.55
28	2009	L'Aquila_Italy	6.3	6.55	552	1.94	3.69
29	2008	Iwate_Japan	6.9	16.96	555	2.36	3.69
30	2008	Iwate_Japan	6.9	11.12	398	3.68	5.32

2.3 Equipment of interest

A motor control center (MCC) (Figure 2-5), which is described as a “very important electrical equipment with low seismic capacity [31],” is selected as the targeted component to be isolated vertically. MCCs control numerous safety-related equipment in NPP. It is assumed that the MCC is attached at the location shown in Figure 2-1. The fundamental frequencies of the MCC in the two horizontal directions and the vertical direction are 5.8, 4.8, and 20 Hz, respectively [32]. The vertical isolation system is introduced between the floor and the MCC.



Figure 2-5: Motor control center (MCC) [32].

2.4 Performance objectives

ASCE 4-16 [33] specifies performance expectations (objectives) for isolated nuclear structures. While objectives are given for design basis earthquake (DBE) and beyond design basis earthquake (BDBE), defined as 150% of DBE level, the objectives address only the horizontal isolation. The commentary of ASCE 4-16 specifically notes this and cites the lack of standard commercially available vertical isolation systems. Due to the lack

of clearly defined and accepted performance criteria for vertical isolation systems, the ASCE 4-16 objectives for horizontal isolation are used in this research for the vertical isolation system. Table 2-3 lists the performance objectives of the isolation system and other structures, systems, and components (SSCs).

Table 2-3: Performance expectations for seismically isolated structure [33]

Item	DBE	BDBE
Isolation system	No damage to the isolation system for DBE shaking.	Greater than 90% probability of the isolation system surviving BDBE shaking without loss of gravity-load capacity.
Other SSCs	Greater than 99% probability that component capacities will not be exceeded.	Greater than 90% probability that component capacities will not be exceeded.

2.4.1 Equipment

Bandyopadhyay and Hofmayer [31] carried out experimental tests on the MCC and found three failure modes: contact chatter voltage drop-out, change of state of starter auxiliary contact, and change of state of starter main contact. The fragility function is computed to find the floor accelerations corresponding to 1% and 10% probability of these failure modes. The capacity of a component is expressed as [34]

$$A = \bar{A} \varepsilon_r = \hat{a} \varepsilon_u \varepsilon_r \tag{10}$$

where A is the random variable of the capacity of the component, \bar{A} is the random variable of the median capacity of the component, \hat{a} is the median of \bar{A} , ε_r and ε_u are lognormally distributed with medians equal to one and standard deviations of β_r and β_u , which are

representative the aleatoric randomness and epistemic uncertainty, respectively. The probability density function of \bar{A} is

$$Q = \Phi \left(\frac{\ln \hat{a} - \ln \bar{a}}{\beta_u} \right) \quad (11)$$

where Q is the probability (confidence level) that \hat{a} exceeds the given value \bar{a} , and Φ is the standard normal distribution function. Rearranging Equation (11) leads to

$$\bar{a} = \hat{a} e^{-\Phi^{-1}(Q)\beta_u} \quad (12)$$

The fragility curve is defined as

$$f = \Phi \left(\frac{\ln a - \ln \bar{a}}{\beta_r} \right) \quad (13)$$

where f is probability of failure of the component and a is the demand. Combining Equation (12) and (13) gives

$$f = \Phi \left(\frac{\ln \frac{a}{\hat{a}} + \Phi^{-1}(Q)\beta_u}{\beta_r} \right) \quad (14)$$

The confidence level parameter is assumed 0.5 here [35]. The recommended parameters of the fragility function for the failure modes found by Bandyopadhyay and Hofmayer [31] are presented in Table 2-4. The Equation (14) is used to draw the fragility curve corresponding to each failure mode. Figure 2-6 shows the fragility curves of the three failure modes of the MCC, where *peak equipment acceleration* is the peak absolute acceleration at the base of equipment. Although these fragility curves are based on a test protocol input motion that is different from the motion the MCC would experience atop

the isolation system in this study, they are used herein in the absence of more appropriate fragility information. The acceleration limits under the two hazard levels are 1.03 g and 1.15 g, respectively, as shown in Figure 2-6. Both limits are based on contact chatter voltage drop-out.

Table 2-4: Fragility parameters of failure modes of the MCC [31]

No	Failure Mode	\hat{a}	β_u	β_r
1	Contact chatter voltage drop-out (CCVD)	1.3	0.20	0.10
2	Change of state of starter auxiliary contact (CSSAC)	1.7	0.17	0.15
3	Change of state of starter main contact (CSSMC)	2.1	0.33	0.07

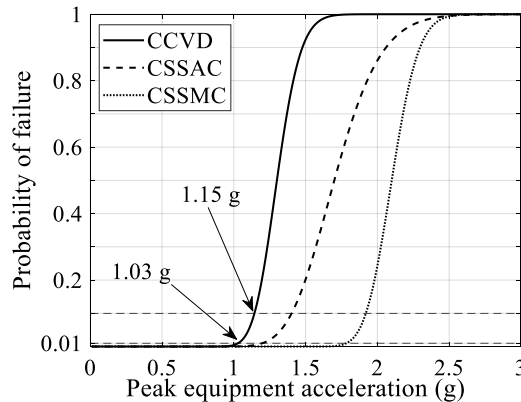


Figure 2-6: The fragility curves of failure modes of MCC: contact chatter voltage drop-out (CCVD), change of state of starter auxiliary contact (CSSAC), and change of state of starter main contact (CSSMC)

2.4.2 Vertical seismic isolation system

To ensure that the isolation system has a 90% probability of surviving the BDBE, the maximum allowable displacement must be found. In the vertical direction, there are three possible failure modes: yielding, pounding, and buckling. The minimum displacement that

causes one of these failure modes is taken as the maximum allowed displacement. As the dispersion of the code response spectrum is unknown, ASCE 4-16 allows the spectrum of the 90th percentile of the BDBE to be calculated by multiplying the DBE spectrum by 3.

2.5 Vertical seismic isolation systems

The MCC is isolated vertically between the floor and the equipment. The equipment is subjected to horizontal and vertical excitation, but the horizontal component of the floor excitation is relatively low because the NPP is horizontally isolated at its base. Therefore, this section focuses on controlling the seismic response of the equipment in the vertical direction only. Three vertical isolation systems are designed to achieve the performance goals outlined in Section 2.4. The three systems consist of in-parallel configurations of linear and nonlinear springs and dampers as follows: (a) linear spring and linear damper (LSLD); (b) linear spring and nonlinear damper (LSND), and (c) nonlinear spring and a linear damper (NSLD). In these systems, the spring and dashpot element are in parallel. For comparing the performances, all these systems are designed such that they are equivalent under the BDBE level. Figure 2-7 and 2-8 show the ground response spectra and the floor response spectra for acceleration and displacement response spectra at the location of the MCC (Figure 2-1) under DBE and BDBE levels, which are used to aid in the design of the vertical isolation systems. The vertical displacement of the LRB does not exceed the cavitation displacement.

The peak ground acceleration in the vertical direction is 1.1 g at the DBE level, which is amplified to 3.0 g at the location of MCC. This large amplification is because the

fundamental frequency of the base isolated NPP (10.42 Hz) in the vertical direction is within the range of large frequency content of the input ground response spectrum. In fact, this amplification will occur regardless of the design of the LRB in the vertical direction. If a very large shape factor is used, the vertical stiffness of the LRB will be very large and the fundamental frequency will be on the order of 20 Hz. If a smaller shape factor is used the vertical stiffness of the LRB will be on the order of 5 Hz; however, if the stiffness is decreased too much, the system will have an issue with rocking. Thus, all feasible LRB designs for horizontal isolation are in the region of the predominant ground motion input frequencies, and as a result there is strong need for vertical isolation of equipment at the floor level.

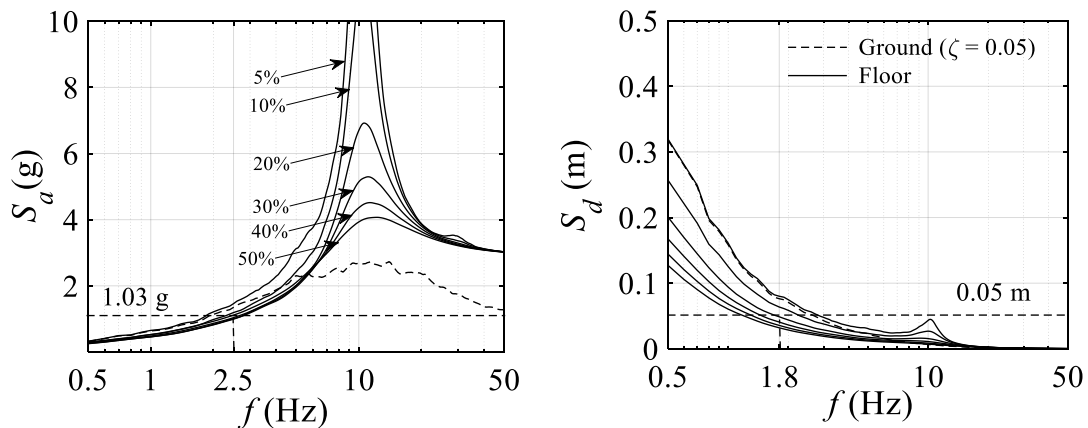


Figure 2-7: (Left) Vertical ground and floor acceleration spectra at the location of the equipment, (right) Vertical ground and floor displacement spectra at the location of the equipment at DBE level (The right figure also shows the displacement demand at 1.8 Hz which is the selected frequency of the LSLD system).

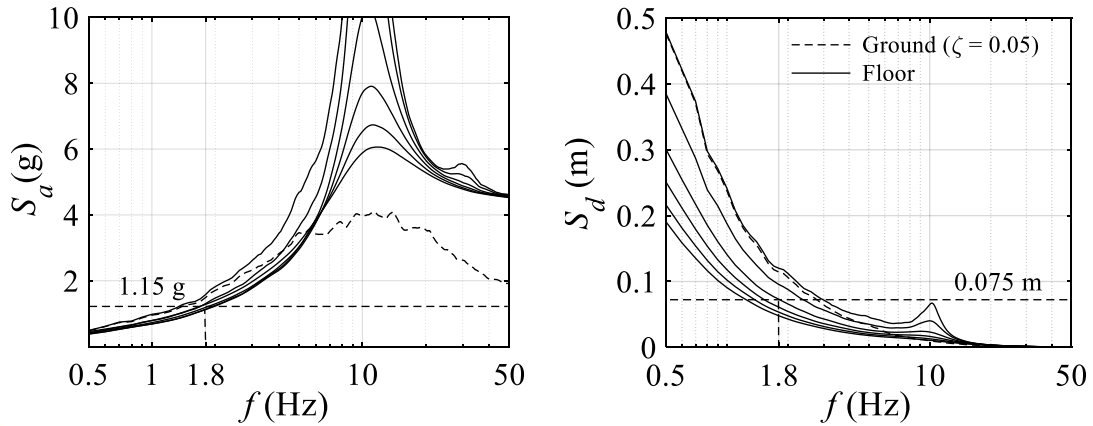


Figure 2-8: (Left) Vertical ground and floor acceleration spectra at the location of the equipment, (right) Vertical ground and floor displacement spectra at the location of the equipment at BDBE level (The right figure also shows the displacement demand at 1.8 Hz which is the selected frequency of the LSLD system).

2.5.1 Linear spring and linear damper

The damping of the LSLD isolation system is chosen to be $\zeta_s = 20\%$ because more damping does not further decrease accelerations (Figure 2-7 (Left)) and has minor impact on displacement (Figure 2-7 (Right)). From Figure 2-7 (Left), to meet the target of 1.03 g spectral acceleration under the DBE level, the vertical isolation system must have a frequency of less than 2.5 Hz. However, to achieve 1.15 g under the BDBE level (Figure 2-8(Left)), the frequency must be less than $f_s = 1.8$ Hz. At this frequency an equipment acceleration of 0.75 g under the DBE level is achieved. Hence, this frequency value is selected for the LSLD system.

The total stiffness of the vertical isolation system is

$$K_t = 4\pi^2 f_s^2 m \quad (15)$$

where $m = 360$ kg is the mass of the MCC. The number of spring (N) is selected 4 and the individual stiffness of each spring is

$$K_i = \frac{K_t}{N} = \frac{G_s d_w^4}{8D_s^3 n_a} \quad (16)$$

where G_s is the shear modulus of steel (79 GPa), d_w is the diameter of the wire, D_s is the diameter of the spring, $n_a = n - 2$ is the number of active coils, and n is the total number of coils.

The mean resulting dynamic displacement demands of the isolation system are 0.05 and 0.075 m under DBE and BDBE levels, respectively (Figure 2-7 and 2-8). The total displacement demand is the summation of the static displacement under gravity and the dynamic displacement. The static displacement can be expressed by

$$u_{\text{stat}} = \frac{g}{4\pi^2 f_s^2} \quad (17)$$

which is 0.075 m for the selected frequency. Consequently, the mean total displacement demands are 0.124 and 0.15 m under the DBE and BDBE levels. Using the assumption of ASCE 4-16 [33], the dynamic displacement demand corresponding to the 90% percentile of the BDBE can be taken as three times the displacement under the DBE (0.05 m) (Table 2-4). Thus, the compressive displacement demand for the vertical isolation system is $u_d = 3 \times 0.05 + 0.075 = 0.22$ m. In tension, the displacement demand is $3 \times 0.048 = 0.14$ m. The displacement capacity of helical springs can be found as [36, 37]

$$u_{max} = \min \left\{ u_y = \frac{\tau \pi D_s^2 n_a}{G_s d_w}, u_b = 0.812 l \left(1 - \sqrt{1 - 6.87 \left(\frac{2D_s}{l} \right)^2} \right), u_l = l - n d \right\} \quad (18)$$

where u_y , u_b , and u_l are the yield displacement, buckling displacement, and free length minus solid length of the spring, τ is the permissible shear stress (550 MPa), and l is the free length of the spring. Equation (18) shows that buckling will not occur when the ratio l/D_s is less than 5.24. Table 2-5 shows the design specifications of the linear spring. The l/D_s for this design is 4.03. Hence, buckling will not occur.

The damping coefficient of the linear damper in the LSLD system is $c_1 = 4\pi m f_s \zeta_s = 1627$ Ns/m.

Table 2-5: Design parameter of each helical spring

Design parameter	Value	Design parameter	Value
G_s (shear modulus of steel)	79 GPa	u_y (yield displacement)	240.19 mm
D_s (mean diameter of spring)	100.8 mm	u_b (buckling displacement)	-
d_w (diameter of wire)	11.1 mm	$u_l (= l - nd)$	251 mm
l (free length)	406.4 mm	u_{max} (displacement capacity)	240.19 mm
n (number of coils)	14	u_d (displacement demand)	220 mm

2.5.2 Linear spring and nonlinear damper

The spring of the LSLD system with frequency 1.8 Hz is used in the LSND system. The seismic design of the nonlinear damper in the LSND system is based on two parameters: the damping ratio ζ_N at each hazard level and the nonlinear exponent parameter α . The typical range of this parameter for seismic isolation is in the range 0.35-1 [38, 39]. The

nonlinear damper with the value of α in the range 1-2 is usually used as shock-absorber [40]. The values of 0.5 and 1.5 are selected for the parameter α in this research. The force of the nonlinear viscous damper, F_D , is expressed by

$$F_D = c_\alpha |\dot{u}|^\alpha \text{sign}(\dot{u}) \quad (19)$$

where c_α is the damping coefficient of the nonlinear damper, and \dot{u} is the velocity. The dissipated energy per cycle of harmonic motion by the linear damper (E_L) and nonlinear damper (E_N) are

$$E_L = c_1 \pi \omega u_0^2 \quad (20)$$

$$E_N = 2\sqrt{\pi} c_\alpha u_0^{\alpha+1} \omega^\alpha \frac{\Gamma\left(1 + \frac{\alpha}{2}\right)}{\Gamma\left(\frac{3}{2} + \frac{\alpha}{2}\right)} \quad (21)$$

where c_1 is the damping coefficient of the linear damper, ω and u_0 are the angular frequency and displacement amplitude of the harmonic motion, and Γ is the gamma function. Equating these two expressions leads to

$$\frac{c_\alpha}{c_1} = \frac{\sqrt{\pi}}{2} (u_0 \omega)^{1-\alpha} \frac{\Gamma\left(\frac{3}{2} + \frac{\alpha}{2}\right)}{\Gamma\left(1 + \frac{\alpha}{2}\right)} \quad (22)$$

and, therefore,

$$c_\alpha = \zeta_s \sqrt{\pi} m \omega^{2-\alpha} u_0^{1-\alpha} \frac{\Gamma\left(\frac{3}{2} + \frac{\alpha}{2}\right)}{\Gamma\left(1 + \frac{\alpha}{2}\right)} \quad (23)$$

where $\zeta_s = 0.2$, $m = 360$ kg, $\omega = 2\pi f_s = 11.304$ s⁻¹ and $u_0 = 0.073$ m. The damping coefficient of the LSND for $\alpha = 0.5$ and 1.5 is 1328 N(s/m)^{0.5} and 1957 N(s/m)^{1.5}, respectively. The equivalent damping ratio at DBE level can be obtained by rearranging Equation (23) and using $u_0 = 0.05$ m. The damping ratio at the DBE level is 0.25 and 0.16 for $\alpha = 0.5$ and $\alpha = 1.5$ (Table 2-6).

2.5.3 Nonlinear spring and linear damper

Nonlinear springs allow the designer to consider different effective frequencies under increasing hazard levels to achieve multiple performance goals. Figure 2-9 shows potential nonlinear springs and their related force-displacement relations. In this figure, d is total displacement (summation of static and dynamic displacement). Wakabayashi et al. [20] proposed a vertical isolation system consisting of V-shaped link with softening behavior. In contrast to V-shaped link springs, conical springs show hardening behavior [41, 42]. The combination of a conical spring and V-link with a gap can achieve softening behavior symmetric centered at the static equilibrium. Cone disk exhibits softening behavior, negative stiffness and hardening behavior. By choosing proper values, the combination of linear spring and cone disk can generate hardening symmetrical behavior centered around the static equilibrium point as proposed by [17, 18].

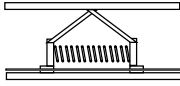
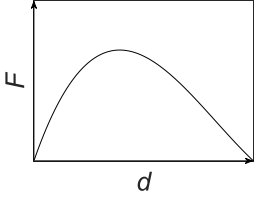
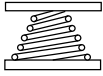
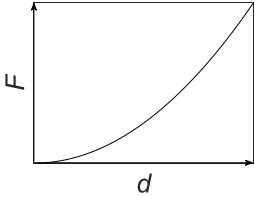
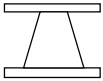
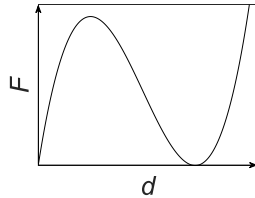
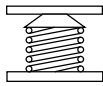
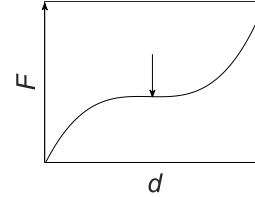
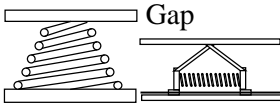
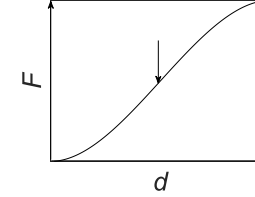
Spring	Schematic View	Force-displacement relation
V-link		
Conical		
Cone disk		
Cone disk + linear		
Conical + V-link		

Figure 2-9: Nonlinear springs configurations with force displacement relation (Black arrows show static equilibrium).

To design the nonlinear spring systems, a bilinear elastic spring is considered with initial stiffness K_1 and secondary stiffness K_2 . The parameters f_1 and ζ_1 are the effective stiffness and damping at the DBE level; similarly, f_2 and ζ_2 are the effective stiffness and damping at the BDBE level. K_1 and K_2 can be expressed by

$$K_1 = 4\pi^2 m f_1^2 \quad (24)$$

$$K_2 = \frac{4\pi^2 m (f_2^2 D_{BDBE} - f_1^2 D_{DBE})}{D_{BDBE} - D_{DBE}} \quad (25)$$

Similar to the LSND system, the effective characteristics $f_2 = 1.8$ Hz and $\zeta_2 = 20\%$ are selected at the BDBE, resulting in a damping coefficient of $c_1 = 4\zeta_2 \pi m f_2 = 1627$ Ns/m. The effective characteristics at the DBE level must achieve an acceleration 1.03 g (Figure 2-7), and because damping coefficient will be constant so that

$$\zeta_1 f_1 = \frac{c_1}{4m\pi} \quad (26)$$

A geometric solution is used to find admissible parameters for the nonlinear spring design. In Figure 2-10, the dotted line shows the possible frequency and damping combinations that will result a peak equipment acceleration of 1.03 g at the DBE level given the response spectra from Figure 2-7. The solid line shows all possible effective characteristics that satisfy Equation (26). The intersection of the two lines leads to effective frequency 2.26 Hz and 15.5%. However, any point on the solid line below the intersection can be a possible solution and should reduce acceleration at the DBE level.

As illustrated in Figure 2-10, if the frequency related to the initial stiffness is larger than 1.8 Hz, the spring shows softening behavior (u is dynamic displacement). If the frequency related to the initial stiffness is smaller than 1.8 Hz, the behavior of spring is hardening. Two separate cases are studied, one with softening and one with hardening behavior: (1) NSLD_S: The frequency at the DBE level is selected to be above 1.8 Hz, as $f_1 = 2$ Hz, which has corresponding $\xi_1 = 18\%$. Substituting these values into Equation (24) and (25) lead to $K_1 = 56791$ N/m and $K_2 = 28659$ N/m. (2) NSLD_H: The frequency at the DBE level is selected to be smaller than 1.8 Hz, as $f_1 = 1.44$ Hz, with corresponding $\xi_1 = 25\%$. The initial and secondary stiffnesses are then $K_1 = 29440$ N/m and $K_2 = 122433$ N/m. The performance of an extreme hardening system, with no initial stiffness as done by [17, 18] is investigated as a separate nonlinear spring and linear damper system, identified as NSLD₀ (Figure 2-11). The NSLD₀ possesses zero stiffness at DBE level and gradually shows hardening behavior to achieve the equivalency point at BDBE level.

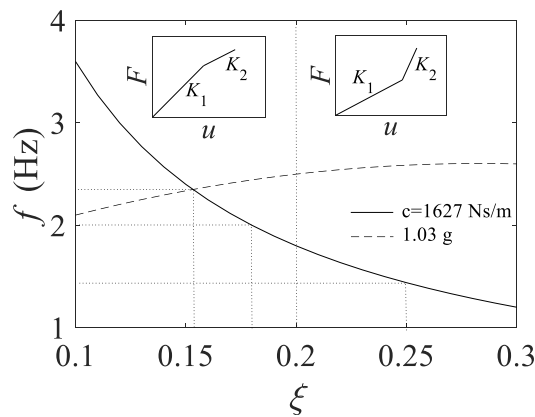


Figure 2-10: Different effective characteristics at DBE level with softening and hardening region

2.6 Results: comparison of the vertical isolation systems

Table 2-6 summarizes the final properties of the six systems, while Figure 2-11 shows the restoring force-displacement behavior of the systems. A decoupled analysis is used to compute the seismic response of the MCC because the mass of the MCC, which is 360 kg, is negligible in comparison to the total mass of superstructure. To compare the performance of the vertical isolation systems, nonlinear time history analysis is conducted using the absolute vertical floor accelerations resulting from the analysis of the horizontally isolated NPP from Section 2.2.3 as input. In this cascading dynamic analysis approach, it is assumed that the dynamic responses of the internal structure of the NPP and the vertical isolated system with the equipment atop it are decoupled. For the purpose of evaluating the performance of the isolation system, it is assumed that the equipment is entirely rigid. This assumption is valid provided that the nominal frequency of the isolation system is well separated from the natural frequency of the equipment. It is noted that even the frequency associated with the first stiffness of the NSLD_H is low and thus is not a cause of concern for resonance in the equipment.

The equation of motion of the isolator–rigid equipment system is

$$m\ddot{u} + c_{\alpha} |\dot{u}|^{\alpha} \text{sign}(\dot{u}) + F = -m\ddot{u}_{fv} \quad (27)$$

where F is the restoring force of the linear or nonlinear elastic spring of the system considered (see Figure 2-11), and \ddot{u}_{fv} is the absolute vertical floor acceleration at the location where the isolator–rigid equipment system is placed (see Fig. 2-1). The resulting absolute acceleration history at the base of the equipment is used to generate the vertical

acceleration response spectra under the DBE and BDBE levels, shown in Figures 2-12 and 2-13 (left), which are used to assess acceleration demands on the isolated equipment. Figures 2-12 and 2-13 (right) show the corresponding maximum displacements of the vertical isolation systems. Table 2-7 summarizes the results of the nonlinear time history analyses of the six systems.

Table 2-6: The design properties of three systems

	K_1 (N/m)	K_2 (N/m)	α	c_α (N(s/m) ^{α})	f (Hz)		ζ	
					DBE	BDBE	DBE	BDBE
LSLD	46000	-	1.0	1627	1.8	1.8	20	20
LSND _{0.5}	46000	-	0.5	1328	1.8	1.8	25	20
LSND _{1.5}	46000	-	1.5	1957	1.8	1.8	16	20
NSLD _S	56791	28659	1.0	1627	2	1.8	18	20
NSLD _H	29440	122433	1.0	1627	1.44	1.8	25	20
NSLD ₀	0	-	1.0	1627	0	1.8	-	20

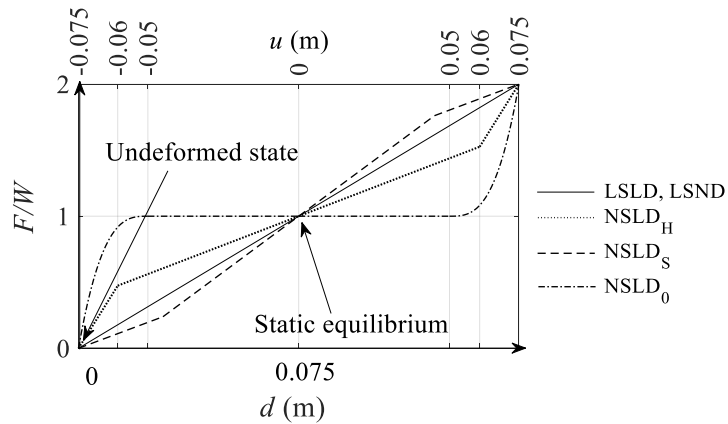


Figure 2-11: Comparison of the elastic spring behavior of the vertical isolation systems (u is dynamic displacement and d is total displacement).

In general, the floor spectra have one peak close to 10 Hz which is the vertical frequency of the of the base isolated NPP. All systems are effective in significantly reducing the peak

equipment acceleration compared to the fixed-base case (i.e., the equipment attached directly to the floor). All of the isolation systems except the NSLD₀ system meet the acceleration performance goal at the DBE level, and all isolation systems are within allowable displacement limits. However, only the LSLD and LSND_{0.5} systems also achieve the acceleration performance target at the BDBE level.

The LSLD system achieves peak equipment accelerations of 0.76 g and 1.14 g under the DBE and BDBE earthquakes, respectively, with mean peak relative displacements of 0.123 m and 0.146 m. The LSND_{0.5} system, with nonlinear damping with value of $\alpha = 0.5$, exhibits marginally smaller peak equipment accelerations than the LSLD system at the DBE level. However, the LSND_{1.5} system meets the acceleration goal at the DBE level but exceeds it at the BDBE level by 2% which can be related to approximation of equivalent linear method.

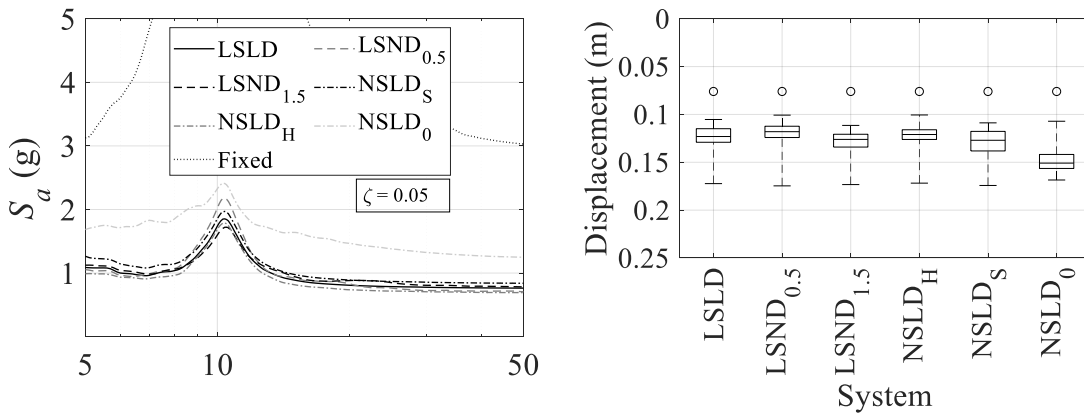


Figure 2-12: Left: Vertical response spectra for the equipment. Right: maximum total displacement of the isolation systems at the DBE level. (Black circles show the static displacement)

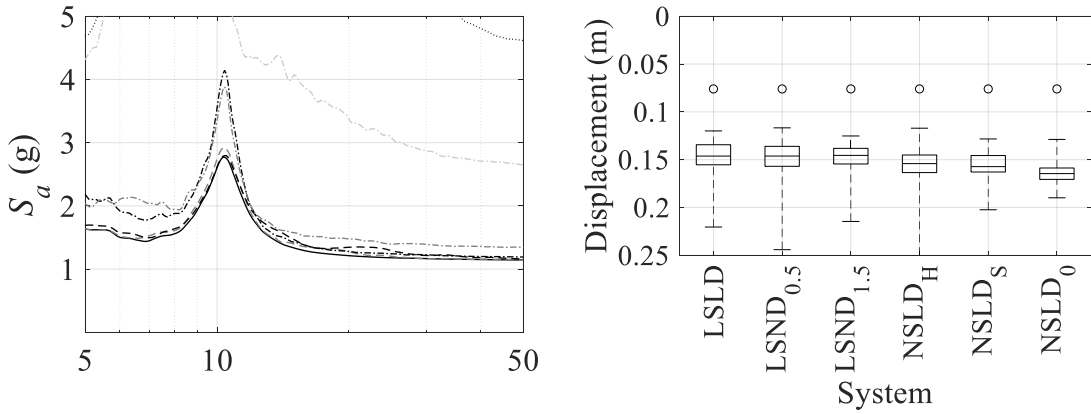


Figure 2-13: Left: Vertical response spectra for the equipment. Right: maximum total displacement of the isolation systems at the BDBE level. (Black circles show the static displacement)

The NSLD_S results in larger accelerations to the LSLD system with similar displacements; and while the NSLD_H results in the lowest value of peak equipment acceleration under the DBE because of the lowest initial frequency, the stiffening behavior under larger displacement causes increased peak equipment accelerations at the BDBE level. The NSLD₀ system exceeds the performance goals at both hazard levels. The system has zero stiffness at the DBE level, but the aggressive hardening after 0.05 m causes very large peak equipment accelerations at both hazard levels. This system also resulted in the largest displacements.

Table 2-7 also shows the average spectral acceleration over the range 5-33 Hz (with increment of 1 Hz) at both hazard levels. This range of frequency is selected as a relevant demand parameter because it encompasses most of the equipment in a NPP [6]. Only the NSLD_H system results in reduced average acceleration relative to the LSLD under the DBE level; however, the NSLD_H acceleration with is considerably higher under the BDBE level.

While the nonlinear damping (LSND_{0.5} and LSND_{1.5}) give average accelerations close to the LSLD, the LSLD provides the best overall performance. In contrast, the NSLD₀ system results in the largest average accelerations due the significant hardening.

Table 2-7: The summary results of the peak base acceleration and the displacement of the four systems. (Bold numbers exceed the performance goal)

	Peak equipment acceleration (g)		Peak isolation displacement (m)		Average spectral acceleration over 5-33 Hz	
	DBE (g)	BDBE (g)	DBE (m)	BDBE (m)	DBE (g)	BDBE (g)
LSLD	0.76	1.14	0.123	0.146	0.93	1.41
LSND _{0.5}	0.71	1.13	0.118	0.146	0.95	1.42
LSND _{1.5}	0.78	1.18	0.126	0.145	0.97	1.49
NSLD _S	0.84	1.19	0.121	0.154	1.02	1.58
NSLD _H	0.69	1.34	0.127	0.157	0.86	1.71
NSLD ₀	1.25	2.65	0.151	0.164	1.57	3.79

2.7 Discussion: Adaptive behavior in horizontal and vertical direction

While adaptive systems have been embraced for horizontal isolation, the results from Section 2.6 have shown that adaptive system may not be appropriate for vertical isolation. Figure 2-14 shows the horizontal ground and vertical floor acceleration and displacement spectra. For horizontal systems, adaptive isolation typically has large initial stiffness to restrict the displacement under wind loading. If the vertical isolation is provided at the base of superstructure, the system might experience rocking motion, requiring provisions to restrict it. In this case, the initial large stiffness in vertical direction is necessary to limit the rotation under low shaking. However, for vertical equipment isolation there is no specific justification to provide this large initial vertical stiffness.

Under moderate shaking, the effective frequency for horizontal isolation is in the range of 0.25 Hz to 0.5 Hz in order to reduce accelerations. However, this can result in large displacement demands, and under very large ground motions excessive displacements rather than accelerations become a concern. Consequently, adaptive horizontal isolation systems can be beneficial to reduce the displacements in large events. In contrast, because of the high frequency content of the vertical floor acceleration (Figure 2-14 (Left)), the frequency of vertical isolation systems can be significantly larger (on the order of 2 Hz). Yet, in general, the displacement demand in the vertical direction is much less than in the horizontal direction (Figure 2-14 (right)). While adaptive systems are beneficial for horizontal base-isolation, a simple spring and viscous damper (linear or nonlinear) can achieve the performance objectives for a vertical equipment isolation system.

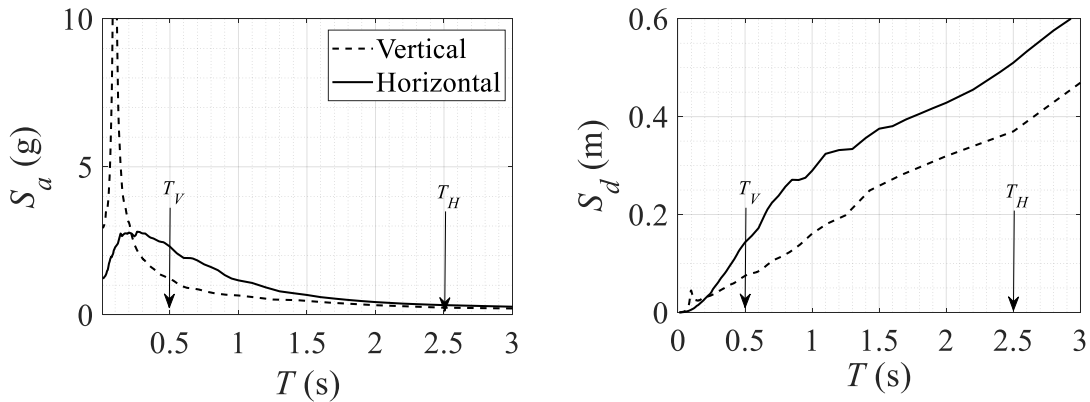


Figure 2-14: (Left) Acceleration spectra and (right) displacement spectra for horizontal direction on the ground and for vertical direction at the location of the MCC. T_H and T_V shows examples of effective horizontal and vertical isolation systems. (The damping ratio is 5%).

2.8 Conclusions

This paper investigated the potential benefits of adaptive vertical equipment isolation for a horizontally base-isolated NPP located in California. Two hazard levels were considered: the DBE with return period 10000 years and the BDBE defined as $1.5 \times \text{DBE}$. A motor control center (MCC), categorized as very important electrical equipment with low seismic capacity, was selected to be vertically isolated. The experimental fragility curve was used to define the engineering demand parameter corresponding to the performance objectives under DBE and BDBE levels for the MCC. Nonlinear dynamic analyses were conducted to compute the floor motions at the location of the MCC. Six isolation systems were considered: linear spring and linear damper (LSLD), linear spring and nonlinear damper with $\alpha = 0.5$ (LSND_{0.5}), linear spring and nonlinear damper with $\alpha = 1.5$, nonlinear spring and linear damper with softening behavior (NSLD_S), nonlinear spring and linear damper with hardening behavior (NSLD_H), and nonlinear spring and linear damper with zero stiffness (NSLD₀). The important observations of this study are summarized as follows:

(1) Equipment at higher levels of the internal structure of NPPs experience large vertical accelerations regardless of the design of LRB due to the high frequency content of vertical component of ground motions. This large amplification justifies the usage of vertical equipment isolation system.

(2) All equipment isolation systems except NSLD₀ system met the acceleration goal at the DBE level. The NSLD_H showed the lowest peak equipment acceleration at DBE level. However, this system did not achieve the acceleration goal at BDBE level. The LSLD and LSND_{0.5} were the only systems that met the acceleration goals under both hazard levels.

(3) All of the equipment isolation systems operated within their allowable displacement limits for the BDBE level. The stiffening regime of the adaptive systems was not necessary because the vertical displacement demands are moderate compared to horizontal displacement demands. Hence, a spring and a damper (linear or nonlinear) can accommodate the displacement demand.

(4) The average spectral acceleration over 5-33 Hz was studied to evaluate the isolation systems to capture the applicability of the system to a wider range of equipment. The results showed that the nonlinear damper had a minor impact on this demand (less than 2%). However, the nonlinear spring increased this demand significantly.

In this study, the equipment was light and small but nuclear power plant houses a large number of equipment with different sizes and weights. It is recommended to study the vertical isolation systems for large and heavy equipment. At least two extra considerations are required for large equipment: (1) The equipment is attached in multiple points and each point may experience different motions. (2) The decoupled analysis is not valid because the weight of the equipment is not negligible in comparison to the superstructure.

References

- [1] Japan Nuclear Energy Safety Organization - JNSE (2013). *JNES-RC-2013-1002: Proposal of Technical Review Guidelines for Structures with Seismic Isolation*, Japan.
- [2] Kumar, M., Whittaker, A. S. and Constantinou, M. C. (2017). "Extreme earthquake response of nuclear power plants isolated using sliding bearings." *Nuclear Engineering and Design*, 316:9-25.
- [3] Zhou, Z., Wong, J. and Mahin, S. (2016). "Potentiality of using vertical and three-dimensional isolation systems in nuclear structures." *Nuclear Engineering and Technology*, 48(5):1237-51.
- [4] Kumar, M., Whittaker, A. S. and Constantinou, M. C. (2015). *Seismic isolation of nuclear power plants using sliding bearings*. Report No. MCEER,
- [5] Huang, Y. N., Whittaker, A. S., Kennedy, R. P. and Mayes, R. L. (2013). "Response of base-isolated nuclear structures for design and beyond-design basis earthquake shaking." *Earthquake Engineering & Structural Dynamics*, 42(3):339-56.
- [6] Huang, Y. N., Whittaker, A. S., Constantinou, M. C. and Malushte, S. (2007). "Seismic demands on secondary systems in base-isolated nuclear power plants." *Earthquake Engineering & Structural Dynamics*, 36(12):1741-61.
- [7] Whittaker, A., Kumar, M. and Constantinou, M. (2015). *Seismic Isolation of Nuclear Power Plants using Elastomeric Bearings*. Report No. MCEER-15-0008, Multidisciplinary Center for Earthquake Engineering Research, University at Buffalo, USA.

- [8] Furukawa, S., Sato, E., Shi, Y., Becker, T. and Nakashima, M. (2013). “Full-scale shaking table test of a base-isolated medical facility subjected to vertical motions.” *Earthquake Engineering & Structural Dynamics*, 42(13):1931-49.
- [9] Guzman Pujols, J. C. and Ryan, K. L. “Computational simulation of slab vibration and horizontal-vertical coupling in a full-scale test bed subjected to 3D shaking at E-Defense.” *Earthquake Engineering & Structural Dynamics*.
- [10] Papazoglou, A. and Elnashai, A. (1996). “Analytical and field evidence of the damaging effect of vertical earthquake ground motion.” *Earthquake Engineering & Structural Dynamics*, 25(10):1109-37.
- [11] Mori, S., Suhara, I., Saruta, M., Okada, K., Tomizawa, T., Tsuyuki, Y., et al. (2012). “Simulation analysis of free vibration test in a building Chisuikan using three-dimensional seismic base isolation system.” *15th World conference on earthquake engineering*, Lisbon, Portugal.
- [12] Nawrotzki, P. and Siepe, D. (2014). “Structural Challenges of power plants in high seismic areas.” *Second European Conference on Earthquake Engineering and Seismology*, Istanbul, Turkey.
- [13] Lee, D. and Constantinou, M. C. (2018). “Combined horizontal–vertical seismic isolation system for high-voltage–power transformers: development, testing and validation.” *Bulletin of Earthquake Engineering*:1-24.
- [14] Medel-Vera, C. and Ji, T. (2015). “Seismic protection technology for nuclear power plants: a systematic review.” *Journal of Nuclear Science and Technology*, 52(5):607-32.

- [15] Morgan, T. A. and Mahin, S. A. (2010). "Achieving reliable seismic performance enhancement using multi-stage friction pendulum isolators." *Earthquake Engineering & Structural Dynamics*, 39(13):1443-61.
- [16] Cimellaro, G. P., Domaneschi, M. and Warn, G. (2018). "Three-Dimensional Base Isolation Using Vertical Negative Stiffness Devices." *Journal of Earthquake Engineering*:1-29.
- [17] Meng, L., Sun, J. and Wu, W. (2015). "Theoretical design and characteristics analysis of a quasi-zero stiffness isolator using a disk spring as negative stiffness element." *Shock and Vibration*, 2015.
- [18] Zhou, Y., Chen, P. and Mosqueda, G. (2019). "Analytical and Numerical Investigation of Quasi-Zero Stiffness Vertical Isolation System." *Journal of Engineering Mechanics*, 145(6):04019035.
- [19] Ueda, M., Ohmata, K., Yamagishi, R. and Yokoo, J. (2007). "Vertical and three-dimensional seismic isolation tables with bilinear spring force characteristics: for which a Λ -shaped link mechanism is used." *Transactions of the Japan Society of Mechanical Engineers, Series C*, 73(735):2932-9.
- [20] Wakabayashi, N., Ohmata, K. and Masuda, T. (2009). "Vertical seismic isolation system using V-shaped link mechanism." *Journal of Japan Society of Mechanical Engineers*, 75:26-32.
- [21] Saady, A. (2017). Personal Communication. Kinetrics Company.
- [22] OpenSees. (2018). Open System for Earthquake Engineering Simulation (Computer software).

- [23] SAP2000. (2016). Static and dynamic finite elements analysis of structures (Computer software).
- [24] Huang, Y.-N., Whittaker, A. S. and Luco, N. (2008). *Performance Assessment of Conventional and Base-Isolated Nuclear Power Plants for Earthquake and Blast Loadings*. Report No. MCEER-08-0019, Multidisciplinary Center for Earthquake Engineering Research, University at Buffalo, USA.
- [25] American Society of Civil Engineers - ASCE (2005). *ASCE/SEI 43-05: Seismic Design Criteria for Structures, Systems, and Components in Nuclear Facilities*, USA.
- [26] Constantinou, M. and McVitty, W. (2015). *Property Modification Factors for Seismic Isolators: Design Guidance for Buildings*. Report No. MCEER-15-0005, Multidisciplinary Center for Earthquake Engineering Research, University at Buffalo, USA.
- [27] Kelly, J. M. and Konstantinidis, D. (2011). *Mechanics of rubber bearings for seismic and vibration isolation*. John Wiley & Sons.
- [28] Constantinou, M., Kartoum, A. and Kelly, J. (1992). "Analysis of compression of hollow circular elastomeric bearings." *Engineering Structures*, 14(2):103-11.
- [29] Gent, A. (1990). "Cavitation in rubber: a cautionary tale." *Rubber Chemistry and Technology*, 63(3):49-53.
- [30] American Society of Civil Engineers - ASCE (2016). *ASCE/SEI 7-16: Minimum Design Loads and Associated Criteria for Buildings and other Structures*, USA.
- [31] Bandyopadhyay, K. and Hofmayer, C. (1986). *Seismic fragility of nuclear power plant components. Phase I*. Report No. NUREG/CR-465g, BNL-NUREG-52007, Vol.2, Brookhaven National Lab., Upton, NY (USA).

- [32] Radford, T. (2015). *Electrical Cabinet Seismic Frequency Estimation*. EPRI Webinar. USA.
- [33] American Society of Civil Engineers - ASCE (2016). *ASCE/SEI 4-16: Seismic Analysis of Safety-Related Nuclear Structures*, USA.
- [34] Kennedy, R. P. and Reed, J. W. (1994). *Methodology for developing seismic fragilities*. Report No. TR-103959, Electric Power Research Institute, California, USA.
- [35] Huang, Y.-N., Whittaker, A. S. and Luco, N. (2011). "A probabilistic seismic risk assessment procedure for nuclear power plants:(II) Application." *Nuclear Engineering and Design*, 241(9):3985-95.
- [36] Shigley, J. E. (2011). *Shigley's mechanical engineering design*. McGraw-Hill Education. USA.
- [37] Becker, L. E. and Cleghorn, W. (1992). "On the buckling of helical compression springs." *International journal of mechanical sciences*, 34(4):275-82.
- [38] Lin, W. H. and Chopra, A. K. (2002). "Earthquake response of elastic SDF systems with non-linear fluid viscous dampers." *Earthquake engineering & structural dynamics*, 31(9):1623-42.
- [39] Asher, J. W., Young, R. P. and Ewing, R. D. (1996). "Seismic isolation design of the San Bernardino county medical center replacement project." *The Structural Design of Tall Buildings*, 5(4):265-79.
- [40] Christopoulos, C. and Filiatrault, A. (2008). *Principles of passive supplemental damping and seismic isolation*. Iuss press. Pavia, Italy.

[41] Rodriguez, E., Paredes, M. and Sartor, M. (2006). “Analytical behavior law for a constant pitch conical compression spring.” *Journal of Mechanical Design*, 128(6):1352-6.

[42] Wu, M. and Hsu, W. (1998). “Modelling the static and dynamic behavior of a conical spring by considering the coil close and damping effects.” *Journal of Sound and Vibration*, 214(1):17-28.

Chapter 3 CONCLUSIONS AND RECOMMENDATIONS

3.1 Summary

This study evaluates the potential benefits of adaptive isolation systems in vertical direction for NPP. To investigate the seismic response in vertical direction and necessity of vertical isolation, a simplified lumped mass stick model of an archetype of NPP was adapted in OpenSees. The location of this model was assumed in California (Diablo Canyon Plant) which is categorized as high seismic risk region. Thirty ground motions are selected and scaled in the horizontal and the vertical directions for return period 10000 years as DBE.

In general, there are three separate approaches in providing three-dimensional isolation. The first approach is to isolate in three direction the whole superstructure at the base. The second approach is to isolate in three directions at floor level. The third approach is to isolate the superstructure at the base horizontally and an acceleration sensitive equipment at the location of item vertically. To overcome the two challenges of three-dimensional isolation at the base of superstructure which are static deflection and rocking motion, the superstructure is isolated horizontally at the base and the acceleration-sensitive equipment is isolated vertically in this research.

Motor control center (MCC) was selected for locally vertical isolation which is categorized as very important electrical equipment with low seismic capacity. The experimental fragility curve was used to define the engineering demand parameter corresponding to the performance objectives under DBE and BDBE levels for the MCC. Nonlinear dynamic analyses were conducted to compute the floor motions at the location of the MCC.

The study investigated six vertical isolation systems: Six isolation systems were considered: (1) linear spring and linear damper (LSLD), linear spring and nonlinear damper with $\alpha=0.5$ (LSND_{0.5}), linear spring and nonlinear damper with $\alpha=1.5$, nonlinear spring and linear damper with softening behavior (NSLD_S), nonlinear spring and linear damper with hardening behavior (NSLD_H) and nonlinear spring and linear damper with zero stiffness (NSLD₀). These systems are designed to meet the multiple performance goals in each hazard levels. For comparison purposes, the adaptive systems are equivalent with LSLD system at DBBE level.

3.2 Conclusion

The results of this research showed that the floors in higher levels of NPP might experience the peak floor acceleration 3 g at DBE level, when the peak ground acceleration is 1.1 g in vertical direction. This large amplification might be related to the closeness of predominant frequency of ground motions and vertical fundamental frequency of superstructure in vertical direction. The research also showed that the superstructure might experience this large amplification in vertical direction and the different design process of horizontal isolation (different shape factor) cannot reduce the vertical response.

The performance of these systems is compared by studying the peak equipment acceleration, relative displacement of isolation system and average spectral acceleration in the range 5-33 Hz.

All equipment isolation systems except NSLD₀ system could meet the acceleration goal at DBE level. The NSLD_H showed the lowest peak equipment acceleration at DBE level.

However, this system could not achieve the acceleration goal at BDBE level. The peak equipment acceleration of LSLD and LSND_{0.5} did not exceed the performance goal at BDBE level.

All equipment isolation systems could achieve the displacement demand at BDBE level. The stiffening regime of adaptive systems for large displacement is not necessary in vertical direction because the displacement demand in vertical direction is much less than horizontal direction. Hence, a spring and a damper (linear or nonlinear) can accommodate the displacement demand.

Average spectral acceleration over 5-33 was studied to evaluate the isolation systems to capture the flexibility of equipment. The results showed that the nonlinear damper had a minor impact on this demand. However, the nonlinear spring increased this demand significantly.

3.3 Recommendation and future study

The following provides some recommendations for future study:

- The large amplification factor of peak floor acceleration in vertical direction justifies the application of supplementary damping devices to mitigate the seismic responses in vertical direction. In this research, the vertical equipment isolation systems were investigated for light items. For future research, it is recommended to study the vertical isolation system of large and heavy equipment. As an example, the steam generator in NPP has 40 m height and it is attached in multiple points. At least two extra consideration should be investigated in this case. The mass of

equipment is not negligible, and a coupled analysis is required to compute the seismic response of equipment. Second, the large equipment is attached in multiple point and each point might experience different seismic response.

- The current accessible experimental fragility curves lack in providing the failure modes and corresponding engineering demands of sensitive equipment in NPP in vertical direction. It is recommended to perform three-dimensional shake table test to define more realistic demands in vertical direction.
- The LRB was used in this research for horizontal isolation of superstructure. The flexibility of the LRB in vertical direction was considered in this research. The different behavior in compression and tension was used to capture the cavitation of rubber in tension. Although the effect of inner hole of the LRB and bulk modulus of rubber on vertical stiffness were modeled in this study, the research neglects the effect of lateral displacement on reduction of vertical stiffness. This reduction might cause larger amplification factor of vertical acceleration. The author suggests investigating this effect on the peak floor acceleration in higher levels.
- This study did not include the contribution of the lead core on the vertical stiffness of the LRB. An analytical model is required to capture this effect. The total vertical stiffness of the LRB might increase with considering the effect of the lead core.
- It is recommended to investigate the amplification of vertical responses, when the TFP system is utilized as horizontal isolation for superstructure. The TFP bearing cannot transfer the tension force. More investigation is needed to study the amplification factor of peak floor acceleration in vertical direction in this case.

APPENDIX A

The coordination of lumped mass nodes and stick model are shown in Table A-1 and A-2. Three translational and three rotational mass of each lumped mass node are presented in Table A-3. The geometric characteristics of beam and column elements are presented in Table A-4. Finally, the beginning and the end node of rigid link element are shown in Table A-5.

Table A-1: Nodes of internal structure (lumped mass)

Node	x (m)	y (m)	z (m)
984	-1.75	-0.01	7
985	1.31	-0.05	12
986	0.12	0	15.4
987	0.09	-0.09	18
988	0.39	10.35	22.88
989	-1.33	-9.99	22.88
990	0.97	10.5	27
991	-0.65	-10.22	27
992	0.95	10.96	30.6
993	0.66	-11.06	30.6
994	1.6	11.48	34
995	1.94	-11.68	34
996	-1.06	12.17	36
997	-0.48	-12.33	36
998	0	13.82	39
999	0.01	-13.83	39

Table A-2: Nodes of internal structure (stick)

Node	x (m)	y (m)	z (m)
1000	0.54	0	0
1001	0.54	0	7
1002	0	0	7
1003	0	0	12
1004	0	0	15.4
1005	0	0	18
1006	0	9.86	18
1007	0	9.86	22.88
1008	0	9.86	27
1009	0	-9.86	18
1010	0	-9.86	22.88
1011	0	-9.86	27
1012	1.36	10.95	27
1013	1.36	10.95	30.6
1014	1.36	10.95	34
1015	1.36	-10.95	27
1016	1.36	-10.95	30.6
1017	1.36	-10.95	34
1018	-1	12.37	34
1019	-1	12.37	36
1020	-1	-12.37	34
1021	-1	-12.37	36
1022	0	13.13	36
1023	0	13.13	39
1024	0	-13.13	36
1025	0	-13.13	39

Table A-3: Three translational and three rotational mass components of each node

Node	U ₁ (kg)	U ₂ (kg)	U ₃ (kg)	M ₁ (kg.m ²)	M ₂ (kg.m ²)	M ₃ (kg.m ²)
984	4077600	4077600	4077600	402000000	396000000	779000000
985	3595780	3595780	3595780	328000000	325000000	666000000
986	2401940	2401940	2401940	223000000	167000000	387000000
987	4793850	4793850	4793850	1170000000	1230000000	770000000
988	1099450	1099450	1099450	213000000	910000000	1090000000
989	1322070	1322070	1322070	225000000	1110000000	1300000000
990	988830	988830	988830	193000000	806000000	980000000
991	1164100	1164100	1164100	192000000	971000000	1140000000
992	763140	763140	763140	121000000	514000000	623000000
993	838510	838510	838510	121000000	561000000	669000000
994	536910	536910	536910	734000000	316000000	383000000
995	619980	619980	619980	769000000	331000000	400000000
996	474670	474670	474670	519000000	279000000	326000000
997	526930	526930	526930	477000000	271000000	314000000
998	309790	309790	309790	183000000	147000000	161000000
999	311390	311390	311390	191000000	502000000	161000000
1000	26355990	26355990	26355990	3440000000	3390000000	5920000000

Table A-4: Geometric characteristics of beams and columns

Element	Node i	Node j	Area (m ²)	J (m ⁴)	I ₂ (m ⁴)	I ₃ (m ⁴)	A _x (m ²)	A _y (m ²)
100	1000	1001	239.35	20323	19553	25026	125.319	110.589
101	1002	1003	263.12	21471	21769	26291	133.36	125.94
102	1003	1004	263.12	21471	21769	26291	133.36	125.94
103	1004	1005	262.13	21183	21417	26560	149.44	108.86
104	1006	1007	84.95	2364.8	8065.1	1756.4	60.08	24.8198
105	1007	1008	84.95	2364.8	8065.1	1756.4	60.08	24.8198
106	1009	1010	84.95	2364.8	8065.1	1756.4	60.08	24.8198
107	1010	1011	84.95	2364.8	8065.1	1756.4	60.08	24.8198
108	1012	1013	71.32	1843	4901.5	1226.2	46.45	24.8201
109	1013	1014	71.32	1843	4901.5	1226.2	46.45	24.8201
110	1015	1016	71.32	1843	4901.5	1226.2	46.45	24.8201
111	1016	1017	71.32	1843	4901.5	1226.2	46.45	24.8201
112	1018	1019	56.25	747.91	3304	617.92	38.5802	17.6198
113	1020	1021	56.25	747.91	3304	617.92	38.5802	17.6198
114	1022	1023	49.05	483.17	2916.5	370.04	38.5798	10.4202
115	1024	1025	49.05	483.17	2916.5	370.04	38.5798	10.4202

Table A-5: Rigid link elements

Rigid link	Node i	Node j
1	984	1001
2	984	1002
3	985	1003
4	986	1004
5	987	1005
6	987	1006
7	987	1009
8	988	1007
9	989	1010
10	990	1008
11	990	1012
12	991	1011
13	991	1015
14	992	1013
15	993	1016
16	994	1014
17	994	1018
18	995	1017
19	995	1020
20	996	1019
21	996	1022
22	997	1021
23	997	1024
24	998	1023
25	999	1025

APPENDIX B

A lead rubber bearing (LRB) system is designed for the horizontal isolation at the base of the NPP with effective period (T_{eff}) and damping (ξ_{eff}) ratio of 2.5 s and 20 %, respectively.

A trial and error process is used to find the characteristics of the LRB. It is assumed that all bearings in the isolation systems are identical. At first, the total number of the LRB is assumed to be $N_b = 150$. The effective stiffness of each isolator is

$$K_{eff} = \frac{4m\pi^2}{T_{eff}^2} \quad (1)$$

where m is the corresponding mass to each isolator

$$m = \frac{M}{N_b} \quad (2)$$

The total mass of the superstructure (M) is 50,000 tons. Substituting the value of $T_{eff} = 2.5$ s gives $K_{eff} = 2.1$ kN/mm . The displacement demand is

$$d = \frac{g}{4\pi^2} \left(\frac{S_a T_{eff}^2}{B} \right) \quad (3)$$

where $S_a = 0.33$ is the spectral acceleration obtained from Figure 2-2 and B is damping modification factor which is [1]

$$B = \left(\frac{\xi_{eff}}{0.05} \right)^{0.3} \quad (4)$$

Equations (3) and (4) gives $d = 0.5$ m. Figure 2-3 shows the force displacement relation of the LRB where K_1 is the initial stiffness, K_2 is the post-yield stiffness, Q_d is the characteristic strength and d_y is the yielding displacement. The equivalent damping ratio is

$$\zeta_{eff} = \frac{W_D}{4\pi E_S} \quad (5)$$

where $W_D = 4Q_d(d - d_y)$ is the dissipated energy per cycle and $E_S = K_{eff}d^2/2$ is the elastic energy stored at the maximum displacement. Rearranging Equation (5) leads to

$$Q_d = \frac{\pi\zeta_{eff}d^2}{2(d - d_y)} \quad (6)$$

The post-yield stiffness is

$$K_2 = K_{eff} - \frac{Q_d}{d} \quad (7)$$

And the yielding displacement is

$$d_y = \frac{Q}{K_1 - K_2} \quad (8)$$

The ratio K_1/K_2 is assumed to be equal to 10 here which is recommended by bearing manufactures [2]. The iterative calculations are shown in Table B-1.

The area of each LRB (A) can be found

$$A = \frac{mg}{\sigma} = \frac{\pi D^2}{4} \quad (9)$$

where $\sigma = 3$ MPa is the static pressure and $D = 1.178$ m is the diameter of the LRB.

The area of the lead core (A_L) is

$$A_L = \frac{Q_d}{\sigma_L} = \frac{\pi D_L^2}{4} \quad (10)$$

Table 0-1: Calculation of design parameters of the LRB

No	d_y (m)	Q_d (N/m)	K_2 (N/m)	d_y (m)
1	0	325034	1442919	0.025
2	0.025	342429	1407572	0.027
3	0.027	343902	1404581	0.027

where $\sigma_L = 8.5\text{MPa}$ is the yield strength of the lead core and $D_L = 0.22$ m. The total thickness of the rubber (t_r) can be found

$$K_2 = f_L \frac{GA}{t_r} \quad (11)$$

where f_L is a parameter for the effect of lead on post-yield stiffness, taken as between 1.0 to 1.2. Here, this parameter is assumed to be 1.1. G is the shear modulus which is equal to 0.4 MPa. Substituting the values of parameters gives $t_r = 0.34$ m. The thickness of each layer (t) is

$$t = \frac{D}{4S} \quad (12)$$

where S is the shape factor which is selected 20. Then, the thickness of each layer is $t = 0.014$ m. The number of layer N_L is as follows

$$N_L = \frac{t_r}{t} \quad (13)$$

which is ended up choosing 25. The total height of the LRB (H) is

$$H = t_r + (N_L - 1)t_s + 2t_b \quad (14)$$

where $t_s = 0.004$ m is the thickness of steel shims and $t_b = 0.05$ m is the thickness of the mounting plates. Then, the total height is 0.56 m.

References

- [1] Ryan, K. L. and Richins, B. (2011). *Design, Analysis, and Seismic Performance of a Hypothetical Seismically Isolated Bridge on Legacy Highway*. Utah Department of Transportation.
- [2] Dynamic Isolation Systems (DIS), “Seismic Isolation for Buildings and Bridges, the Best Earthquake Protection Technology in the World”, *Seismic Isolation Brochure*, Available from <http://www.dis-inc.com/brochures.html> [Accessed 2019].